encit 2020

ABCM Associação Brasileira de Engenharia e Ciências Mecânicas

18th Brazilian Congress of Thermal Sciences and Engineering
November 16-20, 2020 (Online)

ENC-2020-0304
A COMPARATIVE NUMERICAL ANALYSIS OF THE AVAILABLE POWER BETWEEN REGULAR AND IRREGULAR WAVES: CASE STUDY OF AN OSCILLATING WATER COLUMN CONVERTER IN RIO GRANDE COAST, BRAZIL

Gabriel Pereira Tavares
Rafael Pereira Maciel
Elizaldo Domingues dos Santos
Federal University of Rio Grande - FURG, km 8 Itália Avenue, Rio Grande, Brazil
tavares.gabriel95@gmail.com, rafaelmaciel95@hotmail.com, elizaldosantos@furg.br

Mateus das Neves Gomes
Federal Institute of Paraná - IFPR, 453 Antônio Carlos Rodrigues Avenue, Paranaguá, Brazil
mateus.gomes@ifpr.edu.br

Luiz Alberto Oliveira Rocha
University of Vale do Rio dos Sinos - Unisinos, 950 Unisinos Avenue, São Leopoldo, Brazil.
luizor@unisinos.br

Bianca Neves Machado
Federal University of Rio Grande do Sul - UFRGS, km 92, RS-030, 11.700, Tramandaí, Brazil
bianca.machado@ufrgs.br

Phelype Haron Oleinik
Liércio André Isoldi
Federal University of Rio Grande - FURG, km 8 Itália Avenue, Rio Grande, Brazil.
phe.h.o1@gmail.com, liercioisoldi@furg.br

Abstract
Due to the current high cost of production, wave energy is a rather underutilized resource. In order to assess the feasibility and efficiency of installing devices that convert sea wave energy into electrical energy, realistic sea state simulations are of paramount importance. In this context, the present work brings a comparison of the available power in an Oscillating Water Column (OWC) converter device, when subjected to irregular waves (reproducing a realistic sea state) and regular waves (representative of this realistic sea state). The fluid dynamics simulations, performed in the Fluent software, used velocity profiles from the coast of the state of Rio Grande do Sul as boundary conditions for wave generation; these velocity profiles data were obtained from a simulated sea state using the TOMAWAC model. The results show that the average power available in the OWC device is 5 W, obtained with realistic irregular waves. The regular waves representative of the sea state, on the other hand, tend to underestimate the available power by 0.78 times, if calculated based on the peak wave period of the spectrum; and overestimate it by 2.73 times if the mean wave period is adopted for the generation of regular waves. Based on these results, it can be inferred that the peak period would be a more suitable estimator to represent an irregular sea state using regular waves.
Keywords: *sea state, spectrum, irregular waves, numerical modeling.*

1. INTRODUCTION

The increase in energy demand goes hand in hand with society development. As development intensifies, there is a need for greater energy consumption. In this context, renewable energy sources become increasingly relevant (Batlle, 2014).

Sea wave energy stands out in this context, since its total theoretical potential is of the same order of magnitude as the global energy consumption (IEA, 2018). Currently, there are several technologies proposed to convert wave energy into electrical energy. According to Cruz and Sarmento (2004), it is possible to classify the conversion devices

according to the way in which each one converts wave energy into electricity: Overtopping; Oscillating Bodies (point absorbers or surging devices); and Oscillating Water Column (OWC).

Among the mentioned devices, the OWC is the one that stands out the most. It is possible to find several studies on this converter in the literature, such as, Falcão et al. (2012), Simonetti et al. (2017) and Gomes et al. (2018); thus justifying its choice for the analysis developed in the present work.

In addition, the motivation to develop the present work is based on the lack of analysis that use ocean waves realistic data, since most studies use regular waves (e.g., Lopes et al., 2009; Henriques et al., 2012; Elhanafi et al., 2017; Bouali and Larbi, 2017; and Gomes et al., 2017). Therefore, the aim here is to present estimates, closer to reality, about the energy conversion efficiency, performed by the OWC device, considering the region where it would be installed. For this, a coupling between two numerical approaches was performed: the wave generation hydrodynamic model TOMAWAC and the Computational Fluid Dynamics (CFD) commercial code Fluent.

Thus, this article aims to compare the hydropneumatic power available in an OWC type converter device, installed on the coast of Rio Grande-RS, in the south of Brazil, subjected to irregular waves of a realistic sea state and to regular waves representative of this sea state. An OWC converter, with dimensions based on the device located in Pico Island, Azores (Portugal), was then adopted (Pecher et al., 2010).

Hence, from the realistic sea state of the coast of Rio Grande, simulated through the TOMAWAC model, it was possible to determine the wave velocity components, which were imposed as a boundary conditions for the generation of realistic irregular waves in the Fluent software. The OWC device was then subjected to these irregular waves, as well as regular waves representative of that state of the sea.

2. MATERIALS AND METHODS

2.1 Study Area

The case study simulations in this article represented the coast of the city of Rio Grande, in the state of Rio Grande do Sul (RS), Brazil. This region was chosen for its great population concentration, which, according to the 2010 Brazilian Institute of Geography and Statistics (IBGE) census, consisted of 197,228 inhabitants, making it the 10th most populous city in the state, and 1st most populous in the state, when considering the area of cities with direct connection to the sea. Fig. 1 shows the computational domain used in TOMAWAC, where point P represents the region adopted in the case study, located south of Cassino Beach, in the city of Rio Grande, RS, at -52° 17” 47.25’ W, -032° 22” 30.95’ S, with a water depth of 10 m, and 2000 m from the coast, approximately.

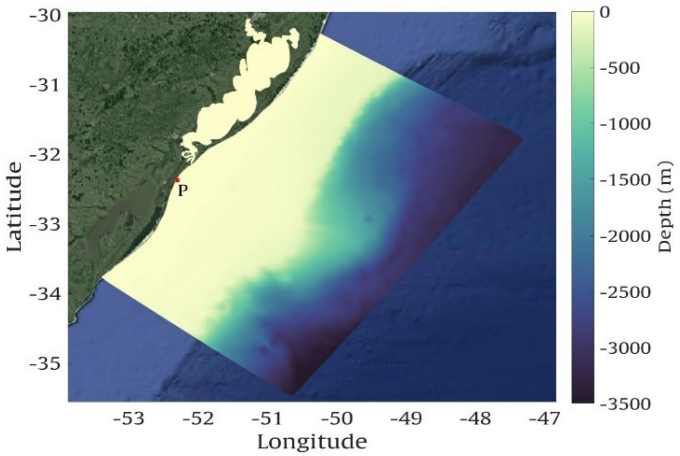

Figure 1. Computational domain used in TOMAWAC for the sea state simulation.

2.2 Computational Models

The methodology adopted in this study required four numerical simulations: the first, with the TOMAWAC model, allowed to obtain a realistic sea state for the study area; and the others, with the Fluent software, allowed to obtain the hydropneumatic power of an OWC device, using: i) the sea state irregular waves; ii) regular waves with the mean wave period (form sea state); and iii) regular waves with peak wave period (from sea state).

TOMAWAC (part of the Open TELEMAC-Mascaret system – www.opentelemac.org) is a third generation spectral wave model. TOMAWAC modeling is based on the balance equation of the wave action density directional spectrum, therefore, the model calculates wind-driven waves, shoaling, whitecapping dissipation, non-linear interactions, and bathymetric breaking. However, TOMAWAC does not take into account reflection and diffraction effects. Thus, this model is not recommended for complex coastal regions (Holthuijsen, 2007). TOMAWAC models the sea state by solving Eq. (1), which expresses a general situation, where waves propagate in a non-homogeneous unsteady medium, in which the wave action density (N) is conserved within the source/sink terms (Q) (Benoit et al., 1996):

$$\frac{\partial N(f,\theta)}{\partial t}+\frac{\partial \dot{x}N}{\partial x}+\frac{\partial \dot{y}N}{\partial y}+\frac{\partial \dot{k}_x}{\partial k_x}+\frac{\partial \dot{k}_y}{\partial k_y}=Q(k_x,k_Y,x,y,t) \tag{1}$$

where N represents the directional spectrum of wave action density, x and y represent the cartesian coordinates system, k_x is the wave number vector component on the x direction and k_y is the y component of the wave number vector, Q is the source term and t is time.

The sea state parameters used in TOMAWAC were obtained from historical data from NOAA's (National Oceanic and Atmospheric Administration) Wave Watch III wave model. The surface wind boundary condition was obtained from NOAA's Reanalysis 1 project, and the bathymetry data used in the seabed representation were obtained through nautical charts from the Directorate of Hydrography and Navigation (DHN), of the Brazilian Navy, and the General Bathymetric Chart of the Oceans (GEBCO). The TOMAWAC simulation was run for a period of 1 year, starting on January 1st, 2014, and ending on December 31st, 2014 (Oleinik et al., 2019).

The Fluent software, on the other hand, was used to solve the governing equations. Fluent is based on the Finite Volume Method (FVM), and it was used to solve the continuity and momentum equations. The multiphase Volume of Fluid (VOF) model was used to tackle with the water-air interaction in the wave flume. In this context, the water free surface can be identified by a variable named volume fraction (f), within each analyzed element in the control volume, it is said that $f = 1$ when the element in question contains only water. When it contains only air, it is considered as $f = 0$, and, in turn, when the element contains both air and water, $0 < f < 1$. In this type of model, there is a certain set of continuity and momentum equations, which are suited for the water-air interaction within a single element. For a Newtonian fluid, the continuity and momentum can be determined by Eqs. (2) and (3), respectively (Hirt and Nichols, 1981; FLUENT, 2007):

$$\frac{\partial \rho}{\partial t}+\nabla(\rho\vec{v})=0 \tag{2}$$

$$\frac{\partial}{\partial t}(\rho\vec{v})+(\rho\vec{v}\vec{v})=-\nabla p+\nabla\left(\bar{\bar{\tau}}\right)+\rho\vec{g} \tag{3}$$

where $\vec{v}$ is the velocity vector, ρ is the density, t is the time, g is the gravitational acceleration, p is the pressure, and $\bar{\bar{\tau}}$ is the surface tension. The volume fraction is modeled by adding Eq. (4) to the system of equations:

$$\frac{\partial(f)}{\partial t}+\nabla(f\vec{v})=0 \tag{4}$$

The physical properties used in Eqs. (2), (3) and (4), assume that:

$$\rho = f\rho_{water}-(1-f)\rho_{air} \tag{5}$$

$$\mu = f\mu_{water}-(1-f)\mu_{air} \tag{6}$$

The coupling between TOMAWAC and Fluent occurs through wave velocities (obtained through TOMAWAC), which are used as prescribed velocity boundary conditions for the generation of irregular waves in Fluent. For this, it is necessary to use the Spec2Wave software, which reads the sea states database generated by TOMAWAC, converting this spectral data into time series of surface elevation and orbital wave velocity, using inverse Fourier transforms.

2.3 Interval of time analyzed

Due to the fact that a wave modeling of this complexity requires great computational power, and for the case study to have maximum representativeness, the delimitation of a time interval that properly represented the characteristics of the sea state in the region was needed. Therefore, a statistical analysis was performed, aiming to estimate the most frequent sea state in the study area.

In this sense, a bivariate histogram of the time series obtained with TOMAWAC (Fig. 2) was made, in order to determine the most frequent combination of significant wave height (H_s) and mean wave period (T_m), so that the simulation represents the largest amount possible of sea conditions at the study area. Therefore, Fig. 2 shows the recurrence of sea states over the analyzed period, where an occurrence of about 2 thousand times was found for a sea state with $H_s \approx 0.66$ m and $T_m \approx 6.30$ s, which represents around 6% of the total in the studied time interval.

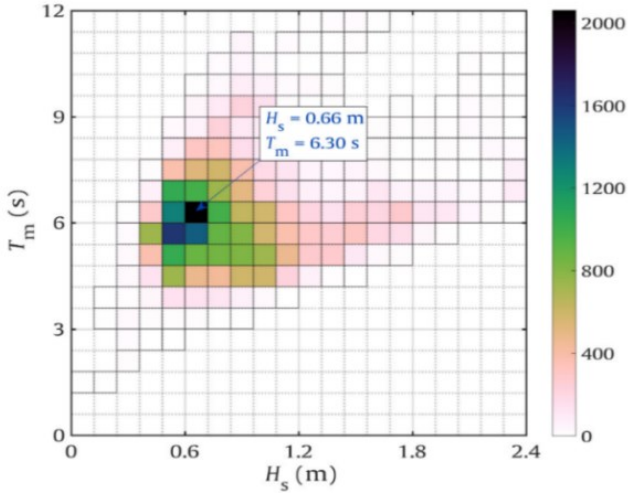

Figure 2. Histogram of wave recurrence, relating T_m e H_s.

Thus, time series of significant height (H_s) and mean period (T_m) were obtained for point P (see Fig. 1), for the year 2014, aiming to estimate realistically the behavior of waves in the region. Fig. 3 shows the time series of Hs and Tm obtained, and the ranges of H_s and T_m selected for analysis.

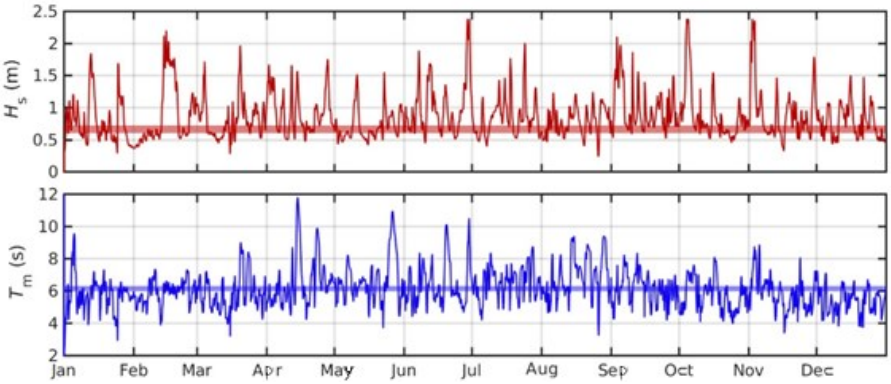

Figure 3. Time series of significant height (H_s) and m period (T_m), on the coast of Rio Grande, in the year 2014.

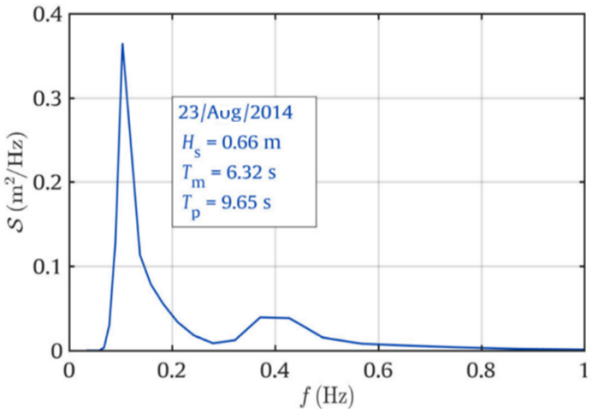

Figure 4. Variance spectrum of representative sea state - I_rB.

Subsequently, several variance spectra present in the year 2014 were observed. Then, the spectrum which came closest to $H_s \approx 0.66$ m and $T_m \approx 6.32$ s was chosen.

After this procedure, a simulation, with a time interval of 15 min, was performed in Fluent, generating irregular waves from the velocity profiles obtained from the spectrum I_rB (Fig. 4).

To determine the irregular waves representing the sea state, it was necessary to convert the surface elevation profile (η) into horizontal and vertical orbital velocity profiles. This allowed these profiles to act as velocity boundary conditions, imposed along the water column at the wave flume entrance.

The wave velocity profiles were determined using Eqs. (7) and (8), obtained by equating the linear wave theory proposed by Airy (1845), and using the deduction made by Holthuijsen (2007), based on the dispersion relation, given by Eq. (9), as follows:

$$u = \omega a \frac{\cosh(k(h+z))}{\sinh(kh)} \cos(kx - \omega t) \tag{7}$$

$$w = \omega a \frac{\sinh(k(h+z))}{\sinh(kh)} \cos(kx - \omega t) \tag{8}$$

$$\omega^2 = gk \tanh(kh) \tag{9}$$

where u and w are the horizontal and vertical wave velocities, respectively, ω is the wave angular frequency, given by $2\pi/T$, k is the wave number, given by $2\pi/L$, z is the position variation between the water free surface and the seabed, a is the wave amplitude, h is the depth, measured from the mean sea level, and g is the gravitational acceleration.

However, not all parameters required for this conversion are known at the moment, so it is necessary to determine the wave angular frequency ω, the amplitude a, and the wave number k. Consequently, ω can be related to the wave period T, and the wave number k can be related to the wavelength L. It is also possible to remove the term kx from the problem, since the surface elevation is given as punctual.

To determine these terms, the zero-up crossing method (Holthuijsen, 2007), widely used in wave record evaluation, was adopted in order to estimate the time interval between the beginning and end of each wave, defined as ΔT. Afterwards, the beginning and end of each obtained wave were marked, so that the interval of each one could be measured, according to Fig. 5.

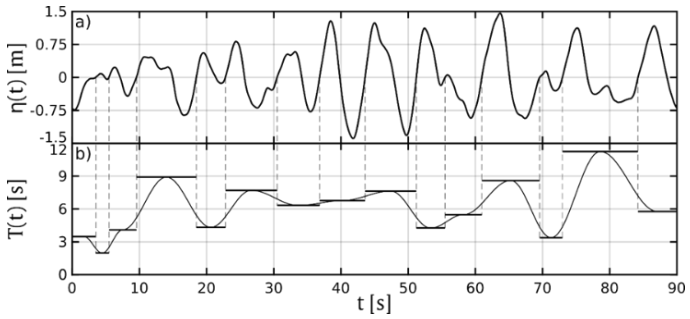

Figure 5. Exemplification of the method used to determine the wave period and the wavelength, through a time series.

After the wave period estimate, the dispersion relation (Eq. (9)) was applied, in order to calculate the length of each wave, resulting in Fig. 6.

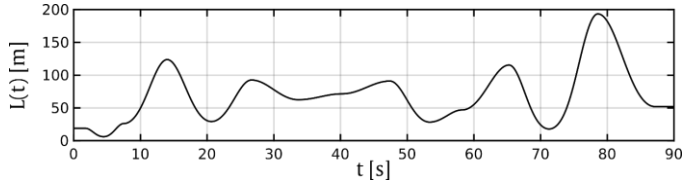

Figure 6. Wavelength, obtained through the application of the dispersion relation.

After all variables have been determined, Eqs. (7) and (8), corresponding to the velocities u and w of wave particles, were used to determine the velocity profiles for irregular waves, obtained from a wave record

2.4 Time and Space Discretizations

Before starting the simulations in Fluent, it was necessary to define, initially, the wave flume dimensions and configurations and, in sequence, the configuration of the adopted mesh. Regarding the wave flume, it was modeled as a rectangular domain, with the upper part open to the atmosphere (atmospheric boundary condition, represented by the dashed green line in Fig. 7), and with the bottom and the right side closed (wall boundary condition, represented by the solid black line in Fig. 7). Thus, the region above the water surface was considered filled with air. In addition, the wave generator can be found on the left side (represented by the red dashed line in Fig. 7), where the velocity profiles x and z directions were imposed, represented, respectively, by u and w (Eqs. 7 and 8).

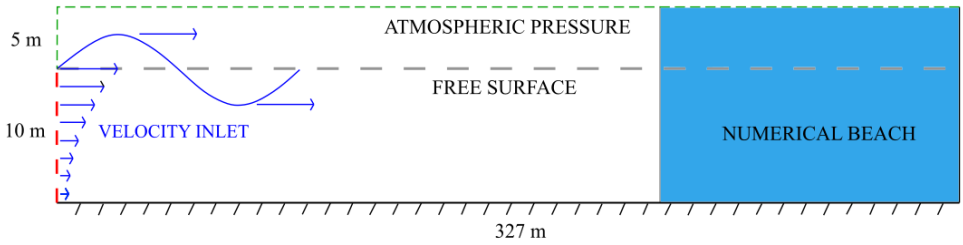

Figure 7. Computational domain of the wave flume used in the numerical simulations.

The wave flume used for the present work was 327 m long and 15 m high, with 10 m being the mean water level. After the wave flume dimensions and boundary conditions were defined, the numerical beach treatment was imposed on the final third of the flume, ranging from 218 m to 327 m. This treatment is essential to prevent incident waves from being reflected by the flume wall, introducing unwanted disturbances in the conversion device that would interfere with the imposed sea state. The numerical beach treatment consists of a region of the channel where an energy sink term that dissipates the waves as they propagate over the region is considered, seeking to reproduce the dissipation that occurs on a real beach (Park et al., 1999).

In order to define a spatial and temporal discretization of the wave channel that allowed the proper generation of irregular waves, mesh convergence and time step tests were performed. To do so, 5 min of propagation of irregular waves were simulated. At first, the spatial discretization of the wavemaker was investigated (dashed line in red in Fig. 7). For that, 18 simulations were performed, varying the area of each mesh element (Δa), the number of divisions (Δv) and the time step between each modeled iteration (Δt), adopting the following values: Δa = {0.2, 0.5}, in m²; Δv = {12, 25, 50}; and Δt = {0.03, 0.05, 0.07} in s.

The results of these simulations showed that the difference between using 15, 25, or 50 divisions on the wavemaker spatial discretization is irrelevant. However, the increase in precision, when using Δv = 25 in comparison to Δv = 15, did not result in an increase in simulation time or in the size of boundary condition files; in contrast, the increase from Δv = 25 to Δv = 50 was rather small, regarding simulation time and file size, but with small significant differences in results. Therefore, Δv = 25 was used in this study.

After defining the spatial discretization of the wave generator, the spatial and temporal discretization of the wave flume were defined. For that, 6 additional simulations were performed, in which Δv = 25; Δa = {0.1, 0.2, 0.5, 0.8}, in m²; and Δt = {0.03, 0.05, 0.07} in s. It was observed that the time step (Δt) had less influence on the results.

To assist in choosing the values of Δa and Δt, the Root Mean Square Error (RMSE) between each simulation considered in the second round of tests and the reference time series was calculated. The RMSE of an X function and the reference E function, both sampled at n discrete points, is calculated according to Chawla et al. (2013):

$$RMSE = \sqrt{\frac{\sum (X - E)^2}{n}} \tag{10}$$

Table 1 presents the RMSE between each of the 12 considered simulations and the reference elevation time series. The additional rows/columns (in bold) show the mean value and percentage difference for each row/column.

Table 1: RMSE for Δt and Δa.

Δt (s) \ Δa (m²)	0.8	0.5	0.2	0.1	$\overline{\Delta a}$	
0.07	0.1717	0.1548	0.1480	0.1454	**0.1550**	
0.05	0.1707	0.1529	0.1459	0.1428	**0.1531**	**-1.23%**
0.03	0.1693	0.1514	0.1443	0.1410	**0.1515**	**-1.02%**
$\overline{\Delta t}$	**0.1706**	**0.1530**	**0.1461**	**0.1431**	Average	
		-10.28%	**-4.55%**	**-2.05%**		Difference

Table 1 shows that, from the simulations using Δa = 0.8 m² to those using Δa = 0.5 m², there was a 10.28% decrease in the calculated RMSE, which represented a considerable improvement in the result. In the case of Δa = 0.2 m², there was a reduction of only 4.55%, and for Δa = 0.1 m², of 2.05%. Table 1 also shows that for simulations with Δt = 0.07 s, compared to those with Δt = 0.05 s, there was a 1.23% reduction in the RMSE, and for Δt = 0.03 s, a reduction of the same order of magnitude, 1.02%. Ideally, the chosen configuration would be the most refined, however there is the computational effort issue. Table 2 shows the processing time for each of these 12 simulations.

Thus, considering the increase of only 20% in the computational effort with the RMSE margins previously presented, the parameter Δa = 0.5 m² was selected for the mesh construction. Likewise, since there is no significant

difference in RMSE between the values of Δt, and taking into account the increase in computational time, the value of $\Delta t = 0.05$ s was chosen for the simulations.

Table 2: Execution time (in h) of each of the 12 simulations performed, and average percentage difference.

Δt (s) \ Δa (m²)	0.8	0.5	0.2	0.1	
0.07	1:14	1:19	3:30	12:26	
0.05	1:25	1:48	4:35	17:20	**30.48%**
0.03	2:12	2:50	7:25	27:20	**58.94%**
		19.91%	**160.74%**	**267.32%**	Difference

With a spatial and temporal discretization that allowed the generation and proper propagation of irregular waves in the wave flume, the next step consisted of inserting the OWC converter into the wave flume.

The OWC dimensions adopted in this study were based on the OWC device installed in Pico Island, Portugal (Pecher et al., 2010), which has a 12 m × 13.4 m hydropneumatic chamber, a 2.7 m × 11.3 m turbine duct, and a submersion depth of 3.4 m. The mesh elements were gradually reduced when approaching the OWC device, aiming to increase precision and reliability of the results. When distancing from device, the elements were gradually returned to the previously predetermined dimensions. The spatial discretizations used in the wave flume and in the device are shown in Fig. 8.

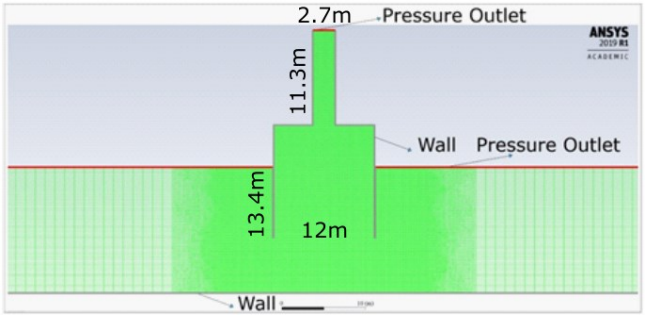

Figure 8. Mesh and boundary conditions in the region around the OWC device.

2.5 Variables of Interest

For the study proposed in this article, numerical probes were defined to monitor the variables of interest during the simulation, as shown in Fig. 9.

Monitors A and B are vertical monitoring lines inserted, respectively, at the beginning of the wave flume ($x = 0$ m) and in the center of the OWC device ($x = 109$ m), being used to measure the free surface elevation (η) over time. Monitor C is a horizontal monitoring line positioned in the center of the turbine duct ($z = 25.65$ m), with the purpose of measuring the mass flow of air throughout the turbine duct. Finally, monitor D, which is a monitoring point located in the center of the turbine duct ($x = 109$ m and $z = 25.65$ m), was used to measure static pressure during the simulation. These numerical probes were positioned according to Gomes et al. (2019).

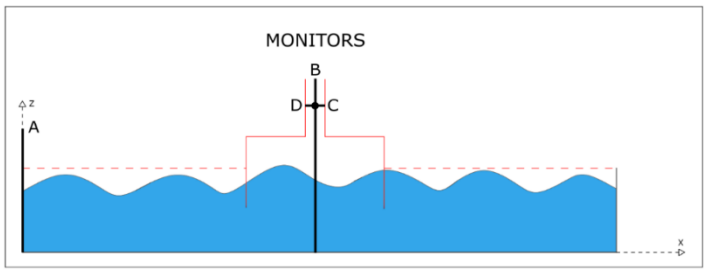

Figure 9. Position of the numerical monitors A, B, C, and D, inserted in the Fluent software.

The calculation of hydropneumatic power, the main variable of interest, is defined by (Dizadji and Sajadian, 2011):

$$P_{hyd} = (P_{air}\frac{\rho_{air}v^2{}_{air}}{2})\frac{\dot{m}}{\rho_{air}} \tag{11}$$

where P_{air} is the static pressure in the turbine duct, ρ_{air} is the air density, $\dot{m}$ is the air mass flow in the turbine duct, and v_{air} is the air velocity in the turbine duct, calculated by (Gomes et al., 2019):

$$v_{air} = \frac{\dot{m}}{A\rho_{air}} \tag{12}$$

where A is the cross-sectional area of the turbine duct, calculated by multiplying the horizontal dimension of the turbine duct (2.7 m, see Fig. 8) by 1 m, since this is a two-dimensional numerical simulation.

As earlier mentioned, the first Fluent simulation was performed with the imposition of irregular waves generated from velocity profiles. After that, two other simulations were carried out; this time, with representative regular waves, based on the parameters obtained through the aforementioned spectrum of variance (Fig. 4). The velocity profiles u and w were obtained through the application of Eqs. (7) and (8), respectively, and were later inserted in Fluent as prescribed velocity boundary conditions. The parameters used for the first regular wave (RT_m) simulated in the wave flume were H_s = 0.66 m and T_m = 6.30 s, and the parameters used for the second regular wave (RT_pB) were H_s = 0.66 m and T_p = 9.65 s.

Figure 10 presents the surface values (η), in m, obtained at the wave flume entrance (monitor A), over the 15 min of irregular waves simulation. The blue line represents the surface elevation obtained through the conversion of the spectrum obtained from TOMAWAC, and the red line corresponds to the surface elevation simulated by Fluent by imposing the boundary conditions (u and w).

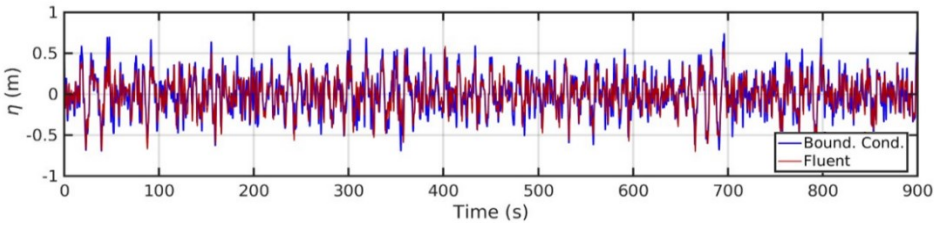

Figure 10. Surface elevation (η) (monitor A, see Fig. 9), over the simulation of 15 min of irregular waves - I_rB.

Thus, it is possible to observe that the waves simulated by Fluent (red line in Fig. 10) have slightly lower peaks than the waves presented by the converted TOMAWAC record (blue line in Fig. 10). Nevertheless, it can be said that, in general, based on Fig. 10, the Fluent simulation is a good representation of the original sea state data. For that, the RMSE of this comparison was calculated, using Eq. (10), obtaining a value of 0.12 m.

Similarly, a comparison of the surface elevation (η) between the two regular waves was performed, as shown in Fig. 11. The blue line is the surface elevation at the entrance of the wave flume, defined by the representative regular wave, obtained through the spectrum of variance (Fig. 4), and the red line corresponds to the surface elevation simulated by Fluent through the imposition of boundary conditions (u and w). Again, waves simulated by Fluent showed a slightly lower peak than the waves obtained by the transformed TOMAWAC record. The RMSE calculated between these comparisons was 0.08 m for RT_pB and 0.04 m for RT_m, using Eq. (10).

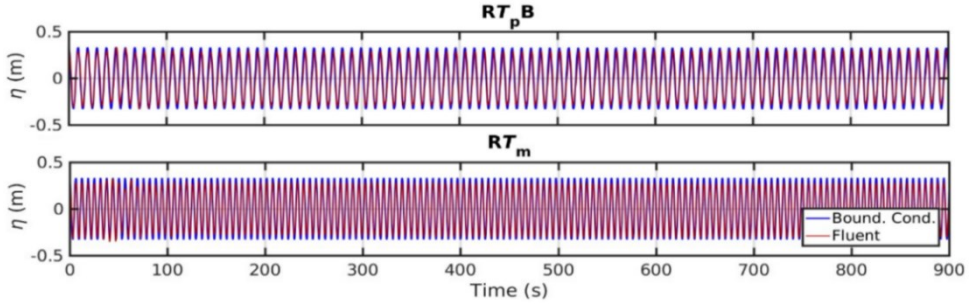

Figure 11. Surface elevation (η) at the wave flume entrance, over the simulation of 15 min of regular waves.

Then, an analysis was performed, comparing the surface elevation at the wave flume entrance (monitor A, see Fig. 9) and in the middle of the OWC device (monitor B, see Fig. 9). The results for both regular waves (RT_pB and RT_m) are presented in Fig. 12. The red line represents the surface elevation at the entrance of the wave flume, and the green line represents the elevation in the middle of the OWC device, over the 15 min simulated by Fluent. Thus, it can be observed, according to Fig. 12, that, as expected, the regular waves propagated continuously through the channel, throughout the simulation. The values of η at the entrance of the channel and in the middle of the device ended up overlapping. The RMSE calculated between these comparisons was 0.05 m for RT_pB and 0.06 m for RT_m, using Eq. (10).

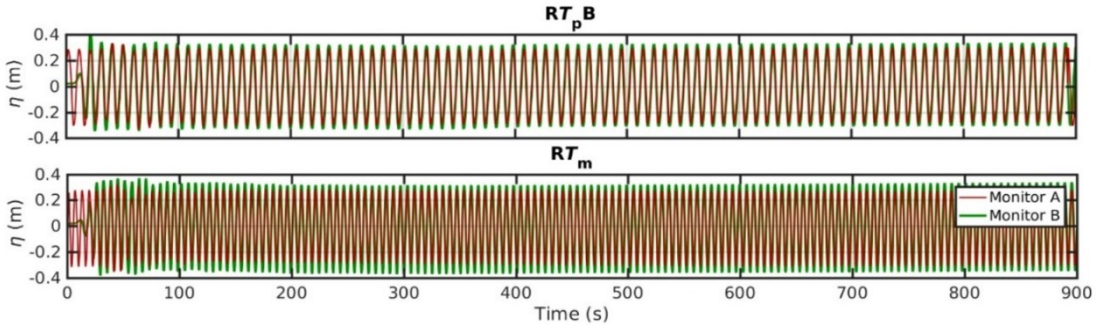

Figure 12. Surface elevation at the entrance of the channel (red line) and in the center of the OWC device (green line), over the simulation 15 min of regular waves.

Finally, an analogous analysis was performed with I_rB irregular waves, comparing the surface elevation (η) at the entrance of the channel (monitor A, see Fig. 9) and at the central point of the OWC device (monitor B, see Fig. 9). However, as the irregular waves propagate at random, it became very difficult to record elevation over the 15 min simulated in Fluent. Therefore, the simulated sea state variance spectrum (Fig. 13) is presented instead of the surface elevation.

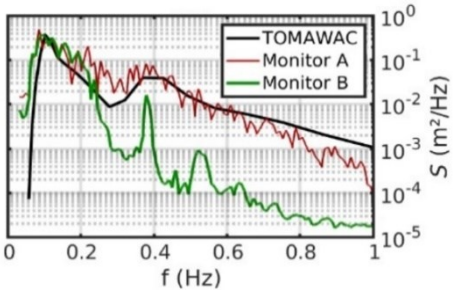

Figure 13. Variance spectrum obtained through TOMAWAC (I_rB), at the entrance of the wave flume (monitor A), and in the center of the OWC device (monitor B).

It can be seen that the spectrum at the input (monitor A, red line) is quite similar to the original spectrum of TOMAWAC, with the exception of some noise level introduced, possibly due to the non-linearity of the fluid dynamics simulation. This shows that the methodology, considering all the steps involved, including obtaining the spectrum, converting it to surface elevation and velocity components, and imposing this data on Fluent, is able to reproduce the original spectrum.

However, 109 m from the beginning of the wave flume, inside the device chamber (monitor B, green line), there is an evident loss of energy in relation to the channel entrance, especially at higher wave frequencies (shorter waves, which indicates that only waves of lesser frequency (f < 0.25 Hz, that is, T > 4 s) are propagated without significant loss. This loss occurs, in part, due to the wave propagation by Fluent itself, and in part, due to the fact that short period waves are reflected by the device wall and have no effect on the surface elevation inside the device, thus explaining the loss and the apparent variance spectrum smoothing observed.

In addition, at the frequency of 0.38 Hz, there is a peak of spectral density in both cases. Because the time series is measured inside the device, this peak may be due to an oscillation inside the device chamber. A more in-depth analysis of the surface elevation behavior inside and outside the device chamber would be needed to better understand the hydrodynamics inside the device.

3. RESULTS

The results regarding the available hydropneumatic power of irregular waves (I_rB) and regular waves (RT_m, RT_pB) are presented here. Figure 14 represents the instantaneous hydropneumatic power available (P_{hyd}), in W, in the turbine duct of the OWC device during the simulated interval of 15 min. For irregular waves (I_rB), a power of 5.12 W was obtained. For the representative regular wave (RT_pB), 4.07 W was obtained, while for the representative regular wave RT_m, 14.17 W was obtained.

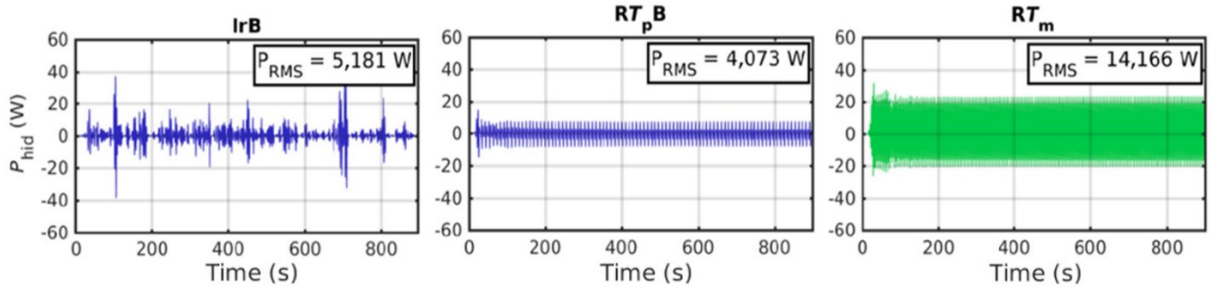

Figure 14. Hydropneumatic power (P_{hyd}) measured in the turbine duct (monitor D, see Fig 8) of the OWC device over the 15 min of simulation.

The difference between the use of the mean period (T_m) and the peak period (T_p) is due to the fact that T_m is, in this case, 3.50 s less than T_p, causing the wave propagation velocity and, consequently, the free surface vertical velocity to be greater for the regular wave with T_m. The mass flow, in turn, can be expressed as a function of velocity (Eq. 12), which makes the hydropneumatic power proportional to the flow velocity raised to the third power. Thus, the difference between T_m and T_p appears as a significant increase in the available hydropneumatic power.

4. CONCLUSIONS

The waves simulated by Fluent through the spectrum transformation, in fact, represented the sea state properly, both for regular and irregular waves. However, during the propagation of irregular waves, there were some losses, possibly due to the numerical method used. Further investigation will be needed to find the source of this dissipation.

Comparing the irregular wave simulation with the two regular wave simulations, the available hydropneumatic power obtained using irregular waves showed a value of around 0.78 times the power obtained from representative regular waves generated from the peak period (T_p). However, for regular waves generated from the mean period of the sea state (T_m) the available power presented a value 2.73 times greater than that obtained with irregular waves.

These results indicate that when using regular waves to represent a sea state to estimate the available hydropneumatic power of an OWC device, the peak period provides, on average, a better estimate than the mean period. However, this result was obtained for a single device geometry, with a single sea state. Further studies are needed to ascertain whether this relationship is valid in more cases.

Therefore, it should be kept in mind that, when performing a simulation of the hydropneumatic power available in an OWC converter device, using regular waves, the period of these waves will directly impact the available power. And, for this estimate to be closer to reality, it is necessary to have information about the sea state of the location where the device would be implanted.

The results obtained show the importance of performing numerical simulations of wave energy converters, more specifically the OWC type, submitted to irregular waves that represent the existing sea state in the region where these devices would be installed, since the analysis made with regular waves can lead to available power values that do not correspond to reality.

5. ACKNOWLEDGEMENTS

The authors thank FURG for the financial support. R. P Maciel and L. A. Isoldi thank to CNPq (*Conselho Nacional de Desenvolvimento Científico e Tecnológico*) for the master research grant (*Chamada* CNPQ/EQUINOR ENERGIA LTDA 2018, Process: 440020/2019-0). P. H. Oleinik thanks to *Coordenação de Aperfeiçoamento de Pessoal de Nível Superior* (CAPES) for his master research grant (Finace Code: 001). The authors L. A. O. Rocha, E. D. dos Santos and L. A. Isoldi thank CNPq for their research grants (Processes: 307791/2019-0, 306024/2017-9, and 306012/2017-0, respectively). The authors also thank to FAPERGS (*Fundação de Amparo à Pesquisa do Rio Grande do Sul*) by the financial support (*Edital* 02/2017 - PqG, Process 17/2551-0001-111-2).

6. REFERENCES

Chawla, A., Spindler, D.M. and Tolman, H.L., 2013. “Validation of a thirty-year wave hindcast using the Climate Forecast System Reanalysis winds”. *Ocean Modelling*, Vol 70, pp.189–206.

Airy, G.B., 1845. *Tides and Waves*. Encyclopedia Metropolitana, pp. 241–396.

Batlle, C., 2014. “Análisis del impacto del incremento de la generación de energía renovable no convencional en los sistemas eléctricos latino-americanos: Herramientas y metodologías de evaluación del futuro de la operación, planificación y expansión”. In *étude de la Banque interaméricaine de développement*. 16 Mar. 2020 <https://publications.iadb.org>.

Benoit, M., Marcos, F. and Becq, F., 1996. "Development of a Third Generation Shallow Water Wave Model with un structured spatial meshing". In *25th International Conference on Coastal Engineering: Book of Abstracts. American Society of Civil Engineers*, pp. 465–478. New York.

Bouali, B. and Larbi, S., 2017. "Sequential optimization and performance prediction of an oscillating water column wave energy converter". *Ocean Engineering*, Vol. 131, pp.162–173.

Cruz, J.M.B.P. and Sarmento, A.J.N.A., 2004. "Energia das Ondas: Introdução aos Aspectos Tecnológicos, Econômicos e Ambientais". *Alfragide: Instituto do Ambiente*.

Dizadji, N., and Sajadian, S.E., 2011. "Modeling and optimization of the chamber of OWC system". *Energy*, Vol. 36, pp. 2360–2366.

Falcão, A.F.O., Henriques, J.C.C., and Cândido, J.J., 2012. "Dynamics and optimization of the OWC spar buoy wave energy converter". *Renewable Energy*, Vol. 48, pp. 369–381.

Fluent, 2007, User's Manual, ANSYS Inc.

Gomes, M. Das N., De Deus, M.J., Dos Santos, E.D., Isoldi, L.A., 2019. "Analysis of the Geometric Constraints Employed in Constructal Design for Oscillating Water Column Devices Submitted to the Wave Spectrum through a Numerical Approach". *Defect and Diffusion Forum*, Vol. 390, pp. 193–210.

Gomes, M.N., Lorenzini, G., Rocha, L.A.O., Dos Santos, E.D. and Isoldi, L.A., 2018. "Constructal Design Applied to the Geometric Evaluation of an Oscillating Water Column Wave Energy Converter Considering Different Real Scale Wave Periods". *Journal of Engineering Thermophysics,* Vol. 27**,** pp. 173–190.

Henriques, J.C.C., Falcão, A.F.O., Gomes, R.P.F., and Gato, L.M.C., 2012. "Latching Control of an OWC Spar-Buoy Wave Energy Converter in Regular Waves". In *Proceedings of the ASME 2012 31st International Conference on Ocean, Offshore and Arctic Engineering*. *Volume 4: Offshore Geotechnics; Ronald W. Yeung Honoring Symposium on Offshore and Ship Hydrodynamics.* Rio de Janeiro, Brazil.

Hirt, C.W., and Nichols, B.D., 1981. "Volume of Fluid (VOF) Method for the Dynamics of Free Boundaries". *Journal of Computational Physics*, Vol. 39, No. 1, pp. 201–225.

Holthuijsen, L. H., 2007. *Waves in Oceanic and Coastal Waters*. Cambridge: Cambridge University Press, 1st edition. UK.

IEA, 2018. Information on http://www.iea.org/. 10 Jul. 2018.

Lopes, M., Ricci, P., Gato, L., and Falcão A.F.O., 2009. "Experimental and numerical analysis of the oscillating water column inside a surface-piercing vertical cylinder in regular waves". In *Proceedings of the 7th European Wave and Tidal Energy Conference (EWTEC).* Porto, Portugal.

Oleinik, P., Kirinus, E., Fragassa, C., Marques, W., and Costi, J., 2019. "Energetic Potential Assessment of Wind-Driven Waves on the South-Southeastern Brazilian Shelf". *Journal of Marine Science and Engineering*, Vol. 7, pp. 1–25. 10.3390/jmse7020025.

Park, J., Kim, M. and Miyata, E.H., 1999. "Fully non-linear free-surface simulations by a 3D viscous numerical wave tank". *International Journal for Numerical Methods in Fluids*, Vol 29, pp. 685–703.

Pecher, A., Kofoed, J.P., Le Crom, I., Neumann, F., and Azevedo, E. De B., 2011. "Performance Assessment of the Pico OWC Power Plant Following the Equimar Methodology". In *Proceedings of the International Offshore and Polar Engineering Conference 2011. International Society of Offshore and Polar Engineers.* pp. 548–556.

Simonetti, I., Cappietti, L., Elsafti, H., and Oumeraci, H., 2017. "Optimization of the geometry and the turbine induced damping for fixed detached and asymmetric OWC devices: A numerical study". *Energy*, Vol. 139, pp. 1197–1209.

7. RESPONSIBILITY NOTICE

The authors are the only responsible for the printed material included in this paper.